Cell, Vol. 92, 713–723, March 20, 1998, Copyright ©1998 by Cell Press

The *Ink4a* Tumor Suppressor Gene Product, $p19^{Arf}$, Interacts with MDM2 and Neutralizes MDM2's Inhibition of p53

Jason Pomerantz,* Nicole Schreiber-Agus,* Nanette J. Liégeois,* Adam Silverman,* Leila Alland,*† Lynda Chin,*‡ Jason Potes,* Ken Chen,* Irene Orlow,§ Han-Woong Lee,*# Carlos Cordon-Cardo,§ and Ronald A. DePinho*‖

*Department of Microbiology and Immunology
†Division of Pediatric Hematology/Oncology
Department of Pediatrics
‡Division of Dermatology, Department of Medicine
Albert Einstein College of Medicine
Bronx, New York 10461
§Department of Pathology
Memorial Sloan-Kettering Cancer Center
1275 York Avenue
New York, New York 10021

Summary

The *INK4a* gene encodes two distinct growth inhibitors—the cyclin-dependent kinase inhibitor $p16^{Ink4a}$, which is a component of the Rb pathway, and the tumor suppressor $p19^{Arf}$, which has been functionally linked to p53. Here we show that $p19^{Arf}$ potently suppresses oncogenic transformation in primary cells and that this function is abrogated when p53 is neutralized by viral oncoproteins and dominant-negative mutants but not by the p53 antagonist MDM2. This finding, coupled with the observations that $p19^{Arf}$ and MDM2 physically interact and that $p19^{Arf}$ blocks MDM2-induced p53 degradation and transactivational silencing, suggests that $p19^{Arf}$ functions mechanistically to prevent MDM2's neutralization of p53. Together, our findings ascribe *INK4a*'s potent tumor suppressor activity to the cooperative actions of its two protein products and their relation to the two central growth control pathways, Rb and p53.

Introduction

Growth control in mammalian cells is accomplished largely by the Rb protein regulating exit from the G1 phase (Weinberg, 1995) and the p53 protein triggering growth arrest/apoptotic processes in response to cellular stress (Levine, 1997). Cross-talk between these two regulatory pathways may be mediated through the p21 cdk inhibitor, which is a target of p53 transactivation as well as a factor that influences the functional status of Rb (Weinberg, 1995). An additional level of overlap between p53 and Rb is provided by the MDM2 protein that can physically associate with both proteins and prevent their growth suppression (Momand et al., 1992; Xiao et al., 1995). In tumorigenesis, Rb and p53 appear to serve collaborative roles as evidenced by the observations that many tumor types exhibit mutations in both *Rb* and *p53* (Williams et al., 1994), and mice that are *Rb* (+/−) and *p53* (−/−) develop a wider range of tumors at earlier ages than mice that are either *Rb* (+/−) or *p53* (−/−) (Williams et al., 1994). Moreover, the ability of several viruses to transform cells in culture and cause tumors in mice is due to viral oncoproteins that bind to and inactivate both Rb and p53 (Mahon et al., 1987; Hawley-Nelson et al., 1989; Munger et al., 1989; Symonds et al., 1994). The mechanistic basis for this dual requirement stems in part from the deactivation of a p53-dependent cell suicide program that would normally be brought about as a response to unchecked cellular proliferation resulting from Rb-deficiency (Gottlieb and Oren, 1996; Ko and Prives, 1996; Levine, 1997).

p53 mutation is thought to be the most frequent genetic alteration in human cancers (Hollstein et al., 1991; Levine et al., 1991). In proliferating normal and neoplastic cells, the consequences of p53 overexpression are context-dependent, resulting in either cell cycle arrest or induction of apoptosis (Ko and Prives, 1996). These biological end points provide a basis for p53's antioncogenic actions (Eliyahu et al., 1989; Finlay et al., 1989) and have been shown to relate to its capacity to function as a sequence-specific transcription factor (Crook et al., 1994; Pietenpol et al., 1994) and to interact with key cellular proteins. The critical role served by p53 in these diverse physiological processes necessitates that p53 activity be subject to stringent multilevel regulation. One crucial level of regulation involves the MDM2 protein, whose direct interaction with p53 blocks p53-mediated transactivation (Chen et al., 1995) and targets the p53 protein for rapid degradation (Haupt et al., 1997; Kubbutat et al., 1997; Levine, 1997). *MDM2* itself has been shown to be amplified in primary tumors (Oliner et al., 1992), to act as an immortalizing oncogene in cell culture (Finlay, 1993), and to directly repress basal transcription (Thut et al., 1997).

In human cancers, disruption of the Rb pathway can result from inactivation of *Rb* itself through gene mutation/deletion, viral sequestration or hyperphosphorylation (Weinberg, 1995), or through disregulation of the components controlling the degree of Rb phosphorylation. The latter can take place through activating mutations in the G1-specific cyclin-dependent kinase 4 (CDK4) catalytic unit, up-regulation of D-type cyclin levels, and/or elimination of *INK4*s (for **in**hibitors of cyclin-dependent **k**inase **4**) (Sherr, 1996). The products of *INK4* family genes have been shown to bind to CDK4 and inhibit CDK4-directed phosphorylation of Rb (Serrano et al., 1993; Quelle et al., 1995a), thereby blocking exit from the G1 phase of the cell cycle (Sherr, 1996). One member of the *INK4* family, *INK4a*, has been shown to exhibit loss of function in a wide spectrum of tumor types; this pathogenetic event appears to be exceeded in frequency only by p53 inactivation. The basis for the prominence of *INK4a*, as opposed to other members of the *INK4* family, in tumor suppression is not fully understood but may relate to its unusual capacity to encode two distinct proteins—the cyclin-dependent kinase inhibitor, $p16^{INK4a}$, and a novel protein of unknown

‖To whom correspondence should be addressed.
#Present address: Department of Biochemistry and Molecular Biology, Seoul National University College of Medicine, Ilchun Institute of Molecular Medicine, Seoul, Korea.

function, p19^{ARF}. This special feature of *INK4a* results from an unusual gene organization in which the two *INK4a* gene products are encoded by different first exons and alternative reading frames residing in a common second exon. The fact that both gene products are often eliminated or mutated in many cancers has raised questions regarding their relative contributions to *INK4a*-mediated tumor suppression.

Compelling support for p16^{INK4a} as a critical target of tumorigenesis includes germline mutations/deletions exclusively affecting the *p16^{INK4a}* ORF in melanoma-prone kindreds and a tumor-associated CDK4 mutation rendering this kinase insensitive to p16^{INK4a} inhibition (Zuo et al., 1996). With regard to p19^{ARF}, although direct evidence linking loss of p19^{ARF} function with human tumorigenesis has been lacking, many *INK4a* mutations/deletions map to the exon 2 region that is shared by *p19^{ARF}*, and a *p19^{ARF}*-specific knockout leads to spontaneous tumor formation in mice (Kamijo et al., 1997).

Some clues addressing p19^{ARF}'s mechanism of action have been provided by the requirement for p53 in p19^{Arf}-induced G1 arrest and by an absence of *p53* mutations in postcrisis *p19^{Arf}* ($-/-$) MEF cultures (Kamijo et al., 1997) and in RAS-induced melanomas arising in the *Ink4a* null mice (Chin et al., 1997). Additionally, studies reported here suggest that p19^{Arf} requires p53 function to suppress cellular transformation. All of these observations have led to the intriguing possibility that the *INK4a* gene is linked not only to the Rb pathway through p16^{INK4a} but also to the p53 pathway through p19^{ARF}. Along these lines, our studies demonstrate that p19^{Arf} engages the p53 pathway through physical interactions with the MDM2 oncoprotein. In addition, we show that p19^{ARF} inhibits the oncogenic actions of MDM2, blocks MDM2-induced degradation of p53, and enhances p53-dependent transactivation. Finally, we demonstrate that loss of *Ink4a* attenuates apoptosis brought about by *Rb* deficiency. These studies provide physical and mechanistic insight fortifying *Ink4a*'s position at the nexus of the two most important tumor suppressor pathways governing the development of neoplasia and provide an explanation for the frequent involvement of *Ink4a* in tumorigenesis.

Results

Distinct and Cooperative Effects of p16^{Ink4a} and p19^{ARF} in the Suppression of Primary Cell Transformation

The antioncogenic potencies of the two *Ink4a* gene products were tested in the rat embryo fibroblast (REF) cotransformation assay (Land et al., 1983) against various oncogene combinations (e.g., *Myc*/*RAS*, *E1a*/*RAS*, or SV40 Large T Antigen (*T-Ag*)/*RAS*). This approach has been used extensively to provide a quantitative measure of antioncogenic activity and allows for placement of these activities along known growth control pathways (Schreiber-Agus et al., 1995; Alland et al., 1997; Lahoz et al., 1997). In the first series of experiments, we investigated the degree of inhibition of *E1a*/*RAS*- versus *Myc*/*RAS*-induced foci formation by *p19^{Arf}*, *p16^{Ink4a}*, or both. As shown in Figure 1, addition of mouse *p16^{Ink4a}* induced a 1.7- to 3-fold reduction in foci number when added to c-*myc*/*RAS* transfections (panel A, p16^{Ink4a}) and failed to cause a statistically significant decrease in *E1a*/*RAS* foci counts (panel B, p16^{Ink4a}); these results are identical to our previous report for the human *p16^{Ink4a}* (Serrano et al., 1995). Since E1A inactivates the Rb protein, the failure of *p16^{Ink4a}* to suppress *E1*/*RAS* transformation is as expected (Lukas et al., 1995; Medema et al., 1995; Serrano et al., 1995). In the same cotransfection experiments, addition of *p19^{Arf}* resulted in marked foci reductions in c-*myc*/*RAS* (5- to 10-fold) as well as *E1a*/*RAS* (4- to 5-fold) cotransfections (panels A and B, p19^{ARF}). *E1a*/*RAS* inhibition by *p19^{Arf}* was not further augmented by the addition of *p16^{Ink4a}* (panel B, compare p19^{Arf} and p16^{Ibk4a} + p19^{Arf}). In contrast, coaddition of *p16^{Ink4a}* and *p19^{Arf}* resulted in a complete inhibition of c-*myc*/*RAS* transformation. Thus, the distinct activity profiles of *p16^{Ink4a}* and *p19^{Arf}* (i.e., *E1a*/*Ras* transfections), together with their additive effects in the c-*myc*/*RAS* transfections, suggests that these proteins suppress neoplasia through separable but cooperative mechanisms of action (see below).

Functional p53 Is Required for Full Oncogenic Suppression by p19^{Arf}

The cell cycle inhibitory effects of p19^{Arf} in primary MEF cultures have been shown to be p53-dependent (Kamijo et al., 1997). To examine the possibility that p19^{Arf} may also act in a p53-dependent manner to suppress cellular transformation, we employed cells rendered functionally (T-Ag or dominant-negative p53) or genetically [*p53* ($-/-$)] deficient for p53 in transformation assays. The addition of *p19^{Arf}* to *T-Ag*/*RAS* cotransfections was found to have no effect on the number of foci generated in the REF assay (Figure 1C) or on the morphological/growth characteristics of these foci (data not shown). Since T-Ag is known to engage many pathways beyond p53 (Fanning, 1992; Van Dyke, 1994), we next assessed the ability of p19^{Arf} to suppress transformation in two other contexts. First, in comparison to the addition of an empty vector control, the addition of *p19^{Arf}* did not affect the number of foci-generated in cotransfections of a dominant-negative mutant form of *p53* (*p53KH215*) and *RAS* in the REF assay (Figure 1C). Second, potent *p19^{Arf}*-induced suppression of *Myc*/*RAS* foci formation was observed in early passage *Ink4a* ($-/-$) mouse embryonic fibroblasts (MEFs), but this suppression was completely eliminated in MEFs doubly null for *Ink4a* and *p53* (Figure 1D). These results strongly suggest that p19^{Arf} does not act in a nonspecific cytotoxic manner to reduce foci formation in the *Myc*/*RAS* and *E1a*/*RAS* experiments described above. Instead, these results appear to assign specificity to the antioncogenic actions of p19^{Arf}. More specifically, in accord with the recently reported cell cycle studies (Kamijo et al., 1997), these findings support the hypothesis that p19^{Arf} acts in a p53-dependent manner to inhibit cellular transformation.

p19^{Arf} Associates with MDM2 In Vivo

To gain insight into the mechanistic basis for the functional link between p19^{Arf} and the p53 pathway, coimmunoprecipitation experiments were performed to assess

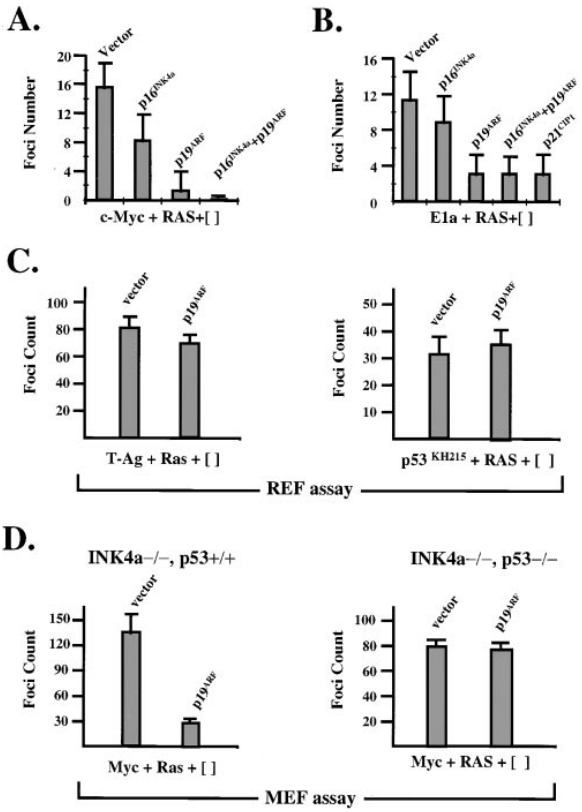

Figure 1. p19Arf Suppression of Transformation in Primary Rodent Cells

(A) Cooperative effects of the mouse *p16Ink4a* and *p19Arf* expression constructs in *Myc/RAS* cotransformation assays. Histogram of a representative REF cotransformation assay showing the average number of foci per 10 cm plate following cotransfections with 2 μg mouse c-*myc*, *H-RAS*^{val12}, and the various expression constructs listed above the error bars.

(B) Distinct actions of *p16Ink4a* and *p19Arf* expression constructs in *E1a/RAS* cotransformation assays. The same experimental design as described in (A) except that each plate was cotransfected with 2 μg E1a, *H-RAS*^{val12}, and the various expression constructs listed. In this particular experiment, the *p16Ink4a* transfection point exhibited an unusually low number of foci relative to the empty vector. Although this decline is not statistically significant, in all other experiments the addition of mouse *p16Ink4a* had no inhibition against *E1a/RAS* transformation, similar to our previous studies with the human *p16Ink4a* (Serrano et al., 1995). Support for the lack of an effect also derives from the lack of additional suppression by *p16Ink4a* in the *p16Ink4a* + *p19Arf* transfection point compared to *p19Arf* alone. The general cyclin-dependent kinase inhibitor p21Cip1 served as a positive control for an inhibitory agent acting downstream of Rb.

(C) Antioncogenic activity of *p19Arf* in T-Ag/RAS or dominant-negative *p53/RAS* REF cotransformation assays. On the left, histogram of a representative REF cotransformation assay showing the average number of foci per 10 cm plate following cotransfections with 2 μg each of *T-Ag*, *H-RAS*^{val12}, and empty vector or *p19Arf*. On the right, histogram showing the average number of foci per 10 cm plate following cotransfections with 2 μg each of *p53KH215* (encoding a dominant-negative mutant p53) and *H-RAS*^{val12} with or without *p19Arf*.

(D) Antioncogenic activity of *p19ARF* in *Myc/RAS* MEF cotransformation assays. The early passage MEFs used for each experiment were either null for *Ink4a* (left panel) or null for both *Ink4a* and *p53* (right panel). The bars represent the number of foci generated in the presence of *p19Arf* relative to control plates receiving 2 μg c-myc, 2 μg *RAS*, and 2 μg empty vector. These assays were performed on an *Ink4a* null background because wild-type MEFs do not give clear, countable foci in *Myc/RAS* cotransformation assays.

potential physical interactions between p19Arf and p53 or the p53-associated protein, MDM2. Since endogenous levels of these proteins are very low in normal primary cells (Levine, 1997), the composition of the p19Arf complexes was determined following cotransfection of various expression constructs (including one encoding a Flag epitope-tagged p19Arf protein, p19Flag) or through the use of different tumor cell lines expressing some or all of these proteins. As shown in Figure 2A, IP-Western blot assays readily detected p19Flag in anti-p53 immunoprecipitates following cotransfection with *p53, MDM2*, and *p19Flag* (lane 2) but not with *p53* and *p19Flag* (lanes 3 and 4). The requirement of MDM2 overexpression to reveal a p53–p19Flag interaction was also observed following either anti-p53 or anti-Flag immunoprecipitations of metabolically labeled transfected cells (data not shown). These results demonstrate that p53, MDM2, and p19Flag can exist as components of a multiprotein complex in vivo. Moreover, the requirement for abundant MDM2 to detect p53–p19Flag interaction suggested that MDM2 serves as a bridging molecule, or that MDM2 induces changes in steady-state levels of p19Flag, among other possibilities. The possibility that MDM2 overexpression stabilizes the level of p19Flag was ruled out by Western blot analysis showing equivalent levels of p19Flag in 293T cells following transfection of MDM2 and p19Flag or of p19Flag alone (data not shown). Moreover, although MDM2 can target p53 for degradation in some cell types (Haupt et al., 1997; Kubbutat et al., 1997), the levels of endogenous p53 in 293T cells remain constant following cotransfection and overexpression of MDM2 (data not shown) due to the presence of T-Ag (Henning et al., 1997).

To examine more directly whether p19Flag can associate with MDM2, coimmunoprecipitation studies were conducted in metabolically labeled 293T cells and in 3T3DM (amplified for Mdm2) and SAOS2 cells (null for p53). In the 293T cells (Figures 2B and 2C), MDM2 was readily detected in anti-Flag immunoprecipitates following cotransfection with *p19Flag* and *MDM2* (lane 8) but not with either empty vector (lane 6), p19Flag alone (lane 5), or MDM2 alone (lane 7). Correspondingly, anti-MDM2 immunoprecipitations confirmed the MDM2–p19Flag association in the *p19Flag* and *MDM2* cotransfections (lane 12). In addition, the endogenous p19Arf band was present in the anti-MDM2 immunoprecipitates (lane 9) and the signal intensity of this band diminished upon cotransfection of *p19Flag* (lane 12), this likely due to competition for a common binding site in the MDM2 complex. In each of these experiments, Western blot analyses of lysates that were run in parallel confirmed the identity of p19Flag and MDM2 bands (data not shown). The interaction between p19Flag and MDM2 in 293T cells was also demonstrated by coimmunoprecipitation in both low- and high-stringency conditions yielding identical results (Figure 2C, lanes 18 and 19, respectively).

To address whether the interaction of T-Ag with MDM2 and p53 (Brown et al., 1993) alters the composition of MDM2/p53/p19Arf complexes in T-Ag-expressing 293T cells, we examined the interaction between endogenous p19Arf and Mdm2 in 3T3DM cell lines. These cells do not express T-Ag but do express high levels of p19Arf (Quelle et al., 1995b) and Mdm2, the latter due to gene amplification (Cahilly-Snyder et al., 1987; Fakharzadeh et al.,

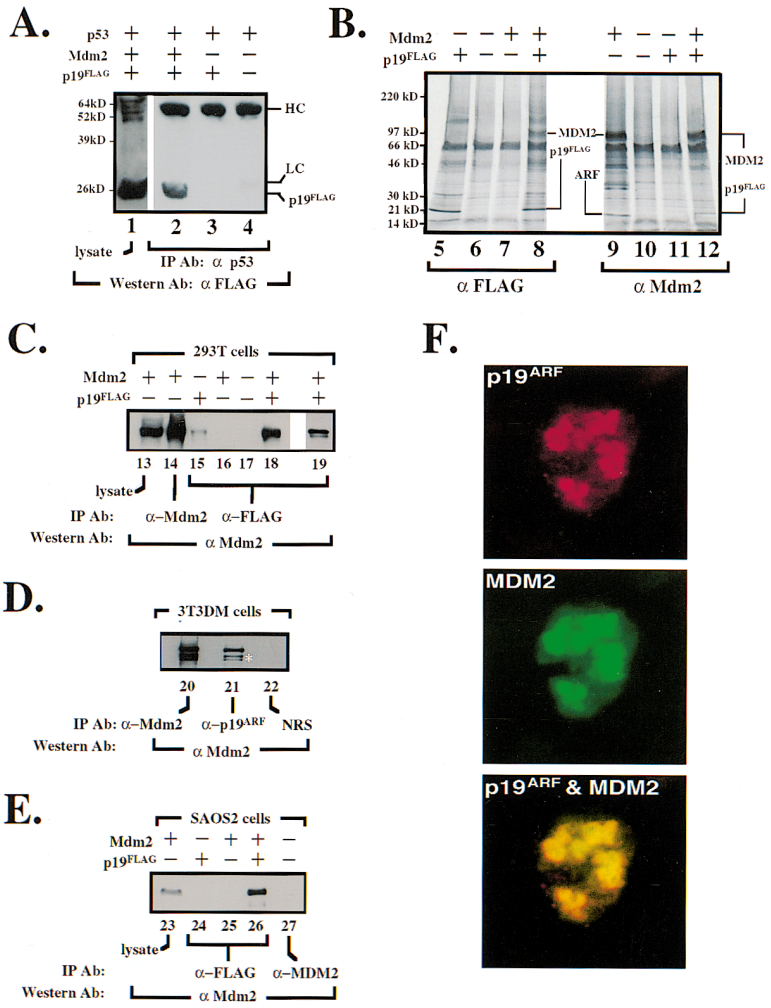

Figure 2. Analysis of the p19^{Arf} Complex In Vivo

(A) Coimmunoprecipitation assay with anti-p53 antibody following transfection of the indicated expression constructs into 293T cells. Western blots were probed with anti-Flag antibody (HC heavy chain, LC light chain) (15% SDS-PAGE).

(B) 293T cells transfected with the indicated expression constructs were metabolically labeled, and immunoprecipitations using anti-Flag (lanes 5–8) or anti-MDM2 (lanes 9–12) antibodies were performed. Precipitated proteins were analyzed on a 4%–15% SDS-PAGE gradient gel.

(C) Immunoprecipitation–Western blot analysis of 293T lysates following transfection with the indicated expression constructs. The lysates were immunoprecipitated with the antibodies indicated below the lanes, and the blots were probed with an anti-MDM2 antibody (8% SDS-PAGE).

(D) Same as (C) except that lysates were derived from untransfected 3T3DM cells, which express high levels of Mdm2, p19^{Arf}, and p53. The asterisk marks the Mdm2 forms that do not interact with p53. The anti-p19^{Arf} is a rabbit polyclonal p19^{Arf} antisera and is compared with nonimmune rabbit serum (NRS) (8% SDS-PAGE).

(E) Same as (C) except that SAOS2 cells were used.

(F) Confocal microscopic analysis of MDM2 and p19^{Arf} protein distribution in 293T nuclei. The yellow signal indicates colocalization of the two proteins. A staining pattern similar to that observed for p19^{Flag} in 293T cells has been observed previously for p19^{Arf} (Quelle et al., 1995b), supporting that this apparent nucleolar localization pattern is not an artifact of overexpression or epitope tagging.

1997). Of note, 3T3DM cells express several alternatively processed species of Mdm2 protein (Figure 2D, lane 20–21, p90/p85, p76/p74, and in very low amounts, p57) (Olson et al., 1993; Barak et al., 1994). Employing a p19^{Arf}-specific antibody for immunoprecipitation, abundant Mdm2 was readily detected upon Western blotting of the immunoprecipitates with anti-Mdm2 antibody (lane 21), further substantiating that p19^{Arf} and Mdm2 interact in vivo. Moreover, the p76/p74 species that lacks the N-terminal p53 binding domain (Olson et al., 1993) is also present in the immunoprecipitates (lane 21, asterisk marks the p76/p74 forms of Mdm2 that do not interact with p53), suggesting that p19^{Arf} can interact with Mdm2 independent of Mdm2's interaction with p53. To confirm this point, anti-Flag immunoprecipitation following cotransfection of *p19^{Flag}* and *MDM2* into *p53* null SAOS2 cells yielded abundant MDM2 signal (Figure 2E, lane 26). Finally, confocal microscopic analysis of the intracellular distribution of each protein demonstrated identical subnuclear localization patterns for p19^{Arf} and MDM2 in both 293T and 3T3DM cells (Figure 2F, 293T cells shown).

Next, a series of plasmids encoding full-length MDM2 or various mutant derivatives was tested for the ability to associate with Flag-tagged p19^{Arf} by coimmunoprecipitation/Western blotting analyses in 293T and SAOS2 cells. The results of these studies, as shown in Figure 3, point to a complex interaction profile in which p19^{Flag} engages multiple sites within MDM2. Specifically, the p19^{Flag}–MDM2 interaction was preserved with deletion of the entire carboxy terminal half of MDM2 (Δ221-491, lanes 12–13), but this interaction was abolished with a slightly larger deletion (Δ155–491, compare lysate in lane 10 to immunoprecipitation in lane 11). While these observations demonstrate an essential role for MDM2 amino acid residues 154–221 in p19^{Arf} binding, an internal deletion mutant of these residues was still capable of p19^{Arf} association in the two cell types (Δ155–221, lanes 6–7 293T, lanes 8–9 SAOS2). The persistent binding of the Δ155–221 mutant may reflect additional points of contact in the carboxyl terminus of MDM2 that cooperate in p19^{Arf} binding. This view is supported by the diminished interaction between p19^{Flag} and the Δ221–491 mutant in SAOS2 cells (compare lanes 12 and 13 to lanes 14 and 15) and also suggests the participation of bridging molecules in 293T that facilitate the p19^{Flag}–MDM2 interaction (e.g., p53, T-Ag, etc.). Taken together, the carboxy-terminal localization, coupled with the ability of a p53-binding-deficient mutant of MDM2 to remain competent for p19^{Arf} binding (lane 1), suggests that p19^{Arf}'s effects upon known properties of MDM2 or p53 (see below) likely do not result from a disruption of the physical

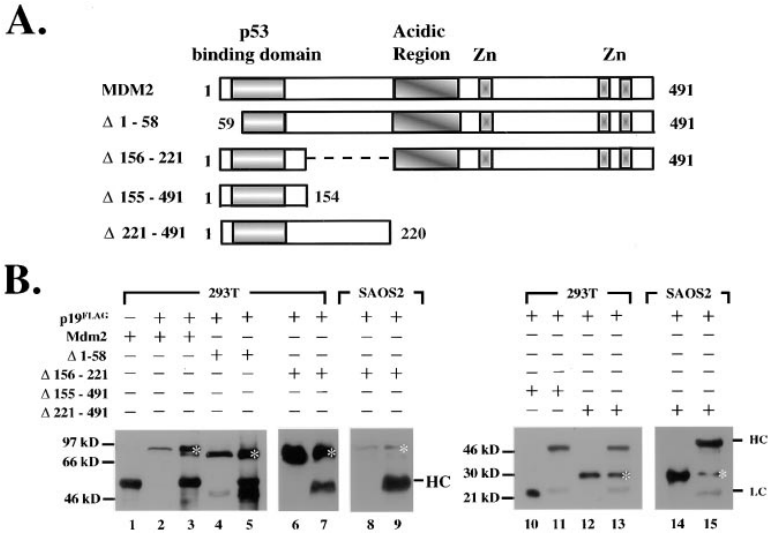

Figure 3. Localization of p19Arf Interaction Region of MDM2

(A) Graphic representation of the full-length MDM2 protein (top) and MDM2 deletion mutants. The known structural motifs and functional domains of MDM2 are indicated. With regard to the Δ1–58 mutant, previous studies have determined that these sequences are essential for MDM2 interaction with p53 (Momand et al., 1992; Oliner et al., 1993; Kussie et al., 1996).

(B) Western blot analysis of lysates (lanes 2, 4, 6, 8, 10, 12, and 14) and of anti-Flag immunoprecipitates (lanes 1, 3, 5, 7, 9, 11, 13, and 15) following transient transfection of the indicated expression constructs into 293T cells (lanes 1–7 and 10–13) or SAOS2 cells (lanes 8–9 and 14–15). Asterisks denote the MDM2 band of interest in each immunoprecipitate. Lanes containing lysate demonstrate that the transfected MDM2 and its mutant derivatives are expressed at high levels. Note the absence of an MDM2 band in the anti-Flag precipitates after transfection of Δ155–491 and p19Flag. The nuclear localization of each mutant protein was confirmed by in situ immunohistochemistry (data not shown). The Western blots were probed with anti-MDM2 monoclonal antibody directed to an epitope (aa 26–168) present within all of the MDM2 proteins used in this assay. Lanes 1–9, 8% SDS-PAGE. Lanes 10–15, 14% SDS-PAGE. HC, heavy chain. LC, light chain.

association between MDM2/p53 by p19Arf. Further support that p19Arf and p53 interact with nonoverlapping regions of MDM2 comes from the observations that p19Arf and p53 can coexist in MDM2 complexes and that p53 immunoprecipitations followed by Western analysis for MDM2 showed similar levels of MDM2 relative to lysate in the presence or absence of p19Arf (data not shown). These conclusions are consistent with data presented in the accompanying paper (Zhang et al., 1998, this issue of *Cell*), which demonstrate that p19ARF can associate with the carboxy-terminal 284 amino acids of MDM2.

Functional Relationship of p19Arf to MDM2 and p53

The physical association between p19Arf and MDM2 establishes a clear connection between a product of the *Ink4a* gene and the p53 pathway. To understand the functional implications of the p19Arf–MDM2 interaction, we assessed the capacity of p19Arf to (1) inhibit MDM2 cotransformation activity, (2) block MDM2-induced degradation of p53, and (3) enhance p53-related activities such as transcription and apoptosis.

Transformation Studies

For the MDM2 transformation studies, we took advantage of the capacity of MDM2 to cooperate with activated RAS to effect the malignant transformation of early passage REFs (Finlay, 1993). In four independent experiments, we observed that the addition of *p19Arf* to *MDM2/RAS* cotransfections resulted in a dramatic reduction in foci numbers, e.g., 40 foci versus 3 foci (Figure 4A). Moreover, compared with *MDM2/RAS* and vector controls, the MDM2/RAS-transformed foci emerging in the *p19Arf* cotransfections exhibited a less transformed morphology (data not shown).

p53 Protein Stability Studies

Next, we examined the consequences of p19Arf overexpression on a key biochemical property of MDM2, namely MDM2's ability to promote the rapid degradation of p53 (Haupt et al., 1997; Kubbutat et al., 1997). For this study, HeLa cells were transiently transfected with the various expression constructs listed in Figure 4B, and the levels of p53 were examined by Western blot analysis. As reported previously (Haupt et al., 1997), p53 steady-state levels were markedly reduced in cells cotransfected with p53 and MDM2 as opposed to p53 alone (Figure 4B, top panel, compare lanes 2 and 3). When *p19Arf* was added to the *p53* + *MDM2* cotransfections, a striking restoration in p53 levels was observed (lane 4). Equal loading of protein was confirmed by reprobing the blots with an anti-Flag antibody, which detects a nonspecific background band (NSFE) (Figure 4B, bottom panel) as well as by Ponceau red staining of blots (data not shown). The precise mechanism through which p19Arf operates to interfere with MDM2-induced degradation is not known. Nevertheless, it is interesting that MDM2 induces a ladder of more slowly migrating bands of p53 (Figure 4C, lane 1), thought to represent ubiquitinated forms of p53 bound for proteasomal degradation (Haupt et al., 1997; Kubbutat et al., 1997). This ladder is significantly reduced in the presence of abundant p19Arf (Figure 4C, lane 2), suggesting that p19Arf inhibits polyubiquitination of p53 triggered by MDM2. Loss of this MDM2-induced ladder was also observed after transfection of p19Arf, p53, and MDM2 into two other cell lines, H1299 and SAOS2 (data not shown). Although our studies strongly suggest that p19Arf blocks MDM2-induced degradation of p53, they do not exclude other possibilities such as p19Arf stabilizing p53 in an MDM2-independent manner.

Regulation of p53 Transactivation Activity

Enforced expression of p19Arf in primary mouse cells results in the induction of *p21Cip1* (a p53-responsive gene; El-Deiry et al., 1993), but only if these cells possess functional p53 (Kamijo et al., 1997; J. P. and R. A. D., unpublished data). These results suggest that p19Arf can enhance the transactivation activity of p53 (Kamijo et al., 1997), perhaps through its ability to counteract MDM2. To test this directly, SAOS2 cells were transfected with a CAT reporter bearing multimerized p53

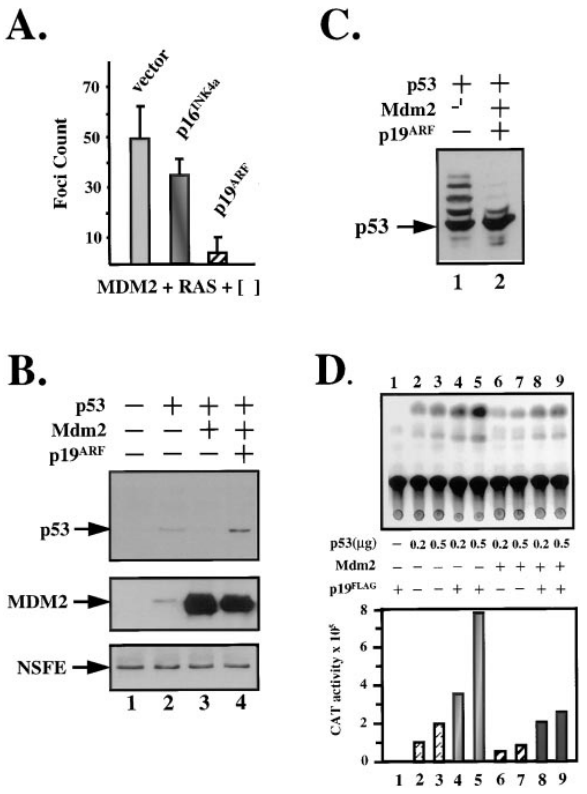

Figure 4. Effect of p19^{ARF} on MDM2-Related Functions

(A) A representative *MDM2/RAS* cotransformation experiment comparing transformed foci counts in *MDM2/RAS* cotransfections receiving either empty vector, *p16^{Ink4a}*, or *p19^{Arf}*.

(B) Top panel, Western blot analysis of HeLa cell lysates probed with anti-p53 antibody (Ab-1 Calbiochem) following transfection of the indicated expression constructs. Middle panel, Western blot of the same lysates probed with an anti-MDM2 antibody. Note induction of endogenous MDM2 upon transfection of p53. The very modest reduction in MDM2 levels observed upon addition of p19^{ARF} (lanes 3 versus 4) is not likely to account for the p19^{ARF} effect since MDM2 levels are greatly increased over those observed in the p53-alone transfections (compare lanes 4 and 2). Bottom panel, Western blot probed with anti-Flag antibody showing a nonspecific cross-reacting Flag epitope (NSFE) used as a loading control.

(C) Higher molecular weight forms of p53 that are induced by MDM2 and thought to represent polyubiquitinated p53 targeted for proteasomal degradation. Note that there is a decrease in these bands upon addition of p19^{Arf}. In this particular experiment, visualization of these p53 bands is facilitated by transfection of higher amounts of p53, use of two different anti-p53 antibodies (DO-1 and 1801), and film overexposure.

(D) Top panel, p53-dependent CAT reporter assays documenting the effects of p19^{ARF}, MDM2, or both on p53 transactivation activity. Amounts loaded are normalized for transfection efficiency. For these SAOS2 transfections, the amounts of DNA used were either 0.2 or 0.5 μg for p53 and 2 μg each for MDM2 or p19^{Arf}. Bottom panel, histogram representation of p53 CAT activities as determined by phosphorimager quantitation of signal intensities.

binding sites in its promoter and with a combination of expression constructs listed in Figure 4D. Since these cells are null for *p53*, CAT activity was detected only in the presence of transfected p53 (compare lane 1 with lanes 2 and 3). Transfection of *p19^{Arf}* resulted in a further increase in reporter gene activity (lanes 4 and 5), an increase that takes place in the presence of detectable endogenous MDM2 levels resulting from exogenous p53 expression (data not shown). As reported previously (Momand et al., 1992; Brown et al., 1993), addition of *MDM2* to the *p53* cotransfections led to a decrease in reporter activity (compare lanes 6 and 7 with lanes 2 and 3), and this effect was abolished with the addition of *p19^{Arf}* (lanes 8 and 9).

In light of the data presented above, enhanced p53 transactivation could result from increased p53 levels due to p19^{Arf}-induced stabilization of p53. However, the findings that overexpression of p19^{Arf} leads to stabilized p53 complexes, which also contain MDM2 (Figure 2), and that MDM2 binds to and masks the p53 transactivation domain raises questions as to how p53 transactivation can be restored by p19^{Arf} in the setting of high levels of MDM2. Among several possibilities are that a subset of transactivation domains in the stabilized p53 tetramer is not bound by MDM2, that p19^{Arf} may function to block MDM2-induced repression of basal transcription, or that p19^{Arf} activates p53 transactivation in an MDM2-independent manner. The resolution of this point will require further analysis in vitro. In summary, these results demonstrate that p19^{Arf} can enhance a key function of p53, its capacity to function as a sequence-specific transcription factor.

Ink4a-Deficiency Attenuates Apoptosis In Vivo

The observed effects of p19^{Arf} on p53 dependent transactivation (this study) and gene expression (Kamijo et al., 1997), and the established importance of p53 in apoptosis prompted us to assess whether loss of p19^{Arf} may affect the degree of apoptosis in vivo. We have shown previously that the developing mouse lens represents an ideal system for such an analysis since loss of *Rb* function therein is associated with unchecked proliferation and apoptosis in lens fiber cells, and this apoptotic response is highly dependent upon *p53* (Morgenbesser et al., 1994). As an indirect assessment of p19^{Arf} effects upon this phenotype, we compared rates of proliferation and apoptosis in embryos singly null for *Rb* or doubly null for *Rb* and *Ink4a*. Since p16^{Ink4a} is believed to be without effect when Rb is absent, the doubly null lenses were taken to be the functional equivalent of *Rb* (−/−), *p19^{Arf}* (−/−) lenses.

Histological analyses of more than 15 *Rb* (−/−) and *Rb* (−/−), *Ink4a* (−/−) lenses revealed a clear increase in the number of nuclei compared with age-matched wild-type lenses (Figure 5A, compare panels b and c with a). Moreover, doubly null lenses had a 25% increase in the number of nuclei over *Rb* (−/−) only lenses. While the lens fiber region of normal or *Ink4a* (−/−) lenses does not exhibit proliferative activity (Morgenbesser et al., 1994) (Figure 5A, panel d, *Ink4a* (−/−) not shown), inappropriate cell cycle progression was confirmed throughout the lens fiber region of *Rb* (−/−) and *Rb* (−/−), *Ink4a* (−/−) lenses by the large number of cells staining positive for 5-bromo-2′-deoxyuridine (BrdU) incorporation (Figure 5A, panels e and f). When normalized to the total number of nuclei, the degree of BrdU incorporation in *Rb* (−/−) and doubly null lens fiber cells was very similar in age-matched lenses (Figure 5B, left panel, $p < 0.001$). In contrast, when lens fiber cell apoptosis

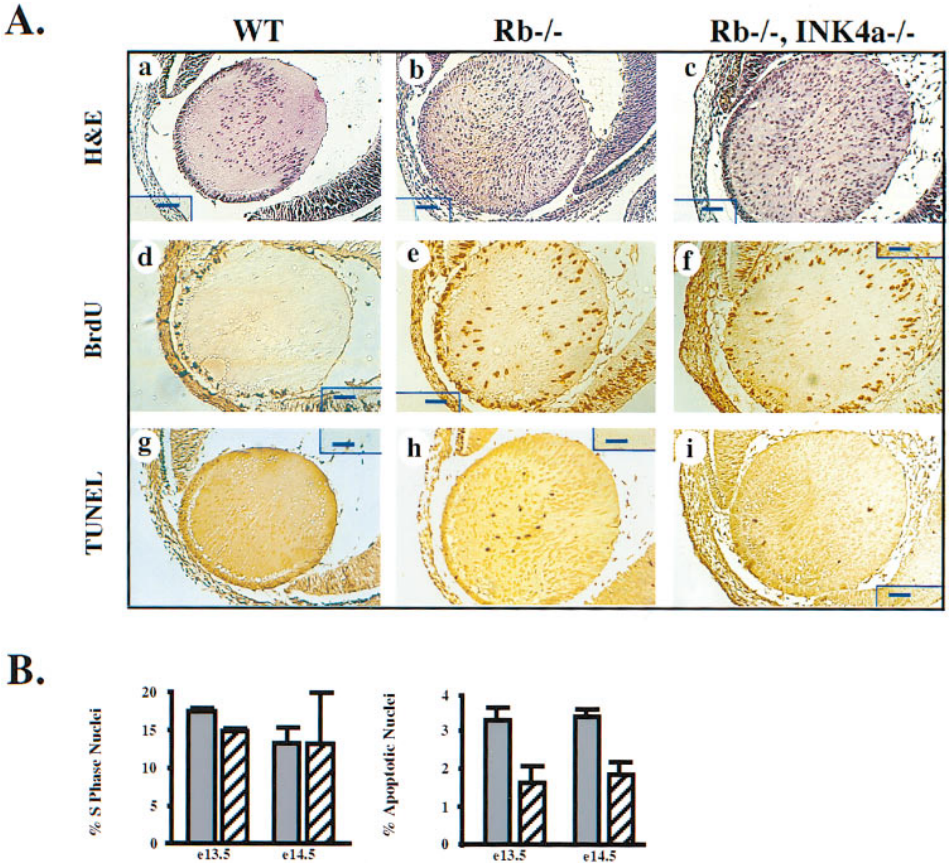

Figure 5. Effect of *Ink4a* Deficiency on Proliferation and Apoptosis in the *Rb*-Deficient Lens In Vivo

(A) Representative sections of age-matched lenses showing morphology by Hand E stain, proliferation by BrdU incorporation, and apoptosis by TUNEL assay in E14.5 wild-type (a, d, and g), *Rb* (−/−) (b, e, and h) and *Rb* (−/−), *Ink4a* (−/−) (c, f, and i) lenses. The lenses are oriented with the anterior epithelium facing the lower left corner and the lens fiber region facing the upper right corner. TUNEL-positive nuclei are stained brown by HRP reaction.

(B) Left panel, quantitative comparision of S phase nuclei (BrdU-positive) relative to the total number of lens fiber nuclei in E13.5 and E14.5 *Rb* (−/−) (closed) and *Rb* (−/−), *Ink4a* (−/−) lenses (striped) (data compiled from examining 332 sections from 19 embryos). Right panel, Quantitative comparision of apoptotic nuclei (TUNEL-positive) relative to the total number of lens fiber nuclei in E13.5 and E14.5 *Rb* (−/−) (closed) and *Rb* (−/−), *Ink4a* (−/−) lenses (striped) (data compiled from examining 174 sections from 13 embryos).

was measured, the number of TUNEL-positive nuclei was significantly and consistently reduced in the doubly null lenses relative to that present in the *Rb*-deficient lenses (Figure 5A, compare panels h and i; Figure 5B, right panel). These studies show that the efficient execution of an apoptotic response known to be dependent upon p53 requires full *Ink4a* gene function. The dual elimination of both *Ink4a* gene products precludes a definitive assignment to $p19^{Arf}$ since it remains theoretically possible that $p16^{Ink4a}$ may play a role in the apoptotic process through an Rb-independent pathway. However, these findings may explain how $p19^{Arf}$ functions as a suppressor of neoplasia, namely through its capacity to enhance the p53-mediated elimination of inappropriately cycling cells in vivo.

Discussion

Recent studies in cell culture and with knockout mouse models have determined that the second product of the *Ink4a* locus, namely $p19^{Arf}$, functions as a potent growth and tumor suppressor that exerts its actions upstream of p53 (Kamijo et al., 1997; Chin et al., 1997; Quelle et al., 1997). Here we refine this connection between $p19^{Arf}$ and the p53 pathway by demonstrating that $p19^{Arf}$ physically associates with MDM2 in vivo and blocks MDM2-induced degradation of p53. The end result of these actions appears to be the enhancement of p53-related functions such as transactivation (reporter assays, Figure 4D), growth inhibition (Kamijo et al., 1997), and possibly apoptosis (lens studies, Figure 5) (see model in Figure 6B). We believe that our studies provide genetic evidence, in addition to physical data, that $p19^{Arf}$ acts primarily on the level of MDM2 rather than p53. The conceptual basis for this argument rests on the fact that although MDM2 overexpression acts to neutralize p53, $p19^{Arf}$ can still inhibit oncogenesis in this setting (Figure 4A). In contrast, other oncoproteins that can neutralize p53 render cells refractory to $p19^{Arf}$ suppression (Figure 1B). Thus, we propose that either (1) $p19^{Arf}$ can interfere with the ability of MDM2 to neutralize p53 (Figure 6B) or (2) $p19^{Arf}$ can affect as yet undetermined MDM2-specific

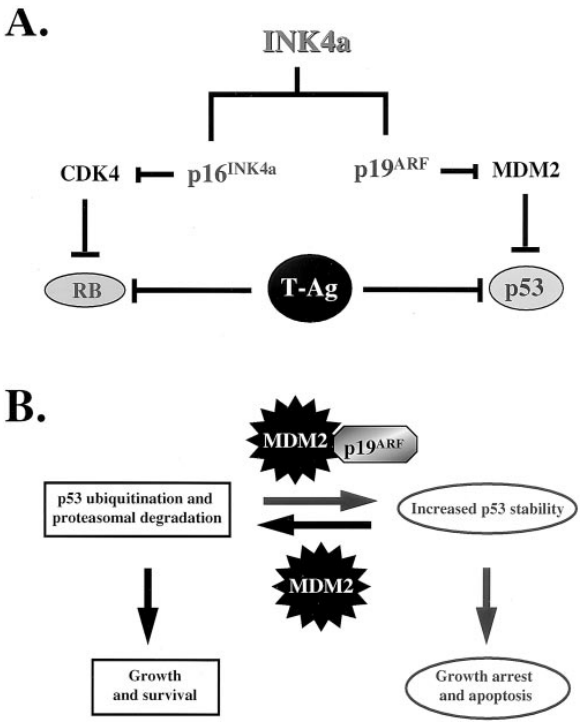

Figure 6. One Gene–Two Products–Two Pathways Hypothesis

(A) Functional relationship of the *INK4a* gene products, $p16^{INK4a}$ and $p19^{ARF}$, and the Rb and p53 tumor suppressors.

(B) Proposed mechanism for $p19^{ARF}$'s enhancement of p53-related functions.

transformation functions beyond those regulating p53 levels and activity. The latter, although formally possible, appears less likely in light of mouse knockout studies suggesting that MDM2 functions primarily (if not exclusively) as a modulator of p53 function (Jones et al., 1995). Regardless of the precise mechanism, the physical and functional link forged between $p19^{Arf}$ and the p53 pathway, along with the previously established one between $p16^{Ink4a}$ and Rb (Serrano et al., 1993; Quelle et al., 1995a) provides for a "one gene–two products–two pathways" hypothesis (Figure 6A) that can explain (1) the exceedingly high rate of *INK4a* gene deletion in many human tumors and their derivative cell lines (Kamb et al., 1994) and in mouse melanomas (Chin et al., 1997) and (2) the strong connection between tumorigenesis and the *INK4a* gene as opposed to other genes encoding cyclin-dependent kinase inhibitors (CKIs), such as *INK4b*, $p21^{CIP1}$, and $p27^{KIP1}$ (Cordon-Cardo, 1995). Specifically, mice lacking *Ink4b* exhibit a very low incidence of spontaneous tumor formation (E. Latres, C. C.-C., and M. Barbacid, unpublished data); $p21^{Cip1}$-deficient mice remain tumor-free (Elledge et al., 1996); and although $p27^{Kip1}$-deficient mice can develop intermediate lobe pituitary hyperplasia or adenoma, these neoplasms rarely progress to malignant pituitary tumors (Elledge et al., 1996). Similarly, in human cancers, the frequent alteration of *INK4a* contrasts sharply with an overall lower rate of *INK4b* mutation/deletion (Cordon-Cardo, 1995) and infrequent mutations in $p21^{CIP1}$ and $p27^{KIP1}$ (Cordon-Cardo, 1995). What makes the *INK4a* gene so unique among the CKIs with respect to tumorigenesis? In essence, two functionally distinct tumor suppressor pathways can be disabled by a single mutational event at the *INK4a* locus, this by virtue of its unusual genetic organization. Stated differently, *INK4a*'s potent tumor suppressor activity likely results from its ability to encode two unrelated antioncogenic proteins with cooperating modes of action (Figure 6A).

Based upon the documented growth-arresting activity encoded by the *INK4a* gene products (Serrano et al., 1993; Quelle et al., 1995b) and the reduction in apoptosis in the lenses doubly null for *Rb* and *Ink4a* (see Figure 5, above), we suggest that the mechanisms of tumor suppression by *INK4a* parallel those established for *Rb* and *p53*. Specifically, the collaborative consequences of loss of $p16^{INK4a}$ and $p19^{ARF}$ are deregulated cell proliferation as well as deactivation or attenuation of p53-dependent apoptosis, which normally serves to promote the efficient elimination of these premalignant cycling cells. In agreement with this hypothesis is the observation that tumors arising in *Ink4a*-deficient mice exhibit high proliferative indices and very low rates of apoptosis despite an intact *p53* gene (C. C.-C. and R. A. D., unpublished data).

One prediction of this hypothesis is that tumors deficient for both $p16^{INK4a}$ and $p19^{ARF}$ would be less likely to harbor *Rb* or *p53* mutations. Furthermore, $p19^{ARF}$-sparing *INK4a* mutations could be associated with alterations involving other components of the p53 pathway (e.g., *MDM2* gene amplification or loss of p53 function). It is important to emphasize that elimination of $p19^{ARF}$ may not preclude p53 mutation since $p19^{ARF}$ tumor suppressor activities are unlikely to overlap fully with those of p53. This lack of equivalence is made evident by the much higher level of genetic instability in p53 (−/−) MEFs compared with Ink4a (−/−) MEFs (Kamijo et al., 1997; N. J. L. and R. A. D., unpublished data) and by the higher rate of spontaneous tumor formation in p53 (−/−) mice versus *Ink4a* (−/−) mice (Jacks, 1994; Serrano et al., 1996). In the lens, the level of reduction in apoptosis achieved with loss of *Ink4a* function was less than that reported previously with loss of p53 (Morgenbesser et al., 1994): reduction of 50%–60% for *Rb* (−/−), *Ink4a* (−/−) versus 75%–85% for *Rb* (−/−), *p53* (−/−). Notwithstanding, loss-of-function mutations of $p19^{ARF}$ would be predicted to decrease the frequency of tumor-associated *p53* mutations. As such, we reexamined reported *INK4a* and *p53* mutations in the same human cancers (Gruis et al., 1995; Newcomb et al., 1995; Brenner et al., 1996; Hangaishi et al., 1996; Heinzel et al., 1996; Kinoshita et al., 1996). These tumor types included melanoma, carcinomas (bladder, oral, and lung carcinomas), and various lymphoid neoplasms (B-cell chronic lymphocytic leukemia, and Hodgkin's and Non-Hodgkin's lymphomas). This analysis demonstrated a reciprocal relationship between p53 and $p19^{ARF}$ mutational events, as *INK4a*-deficient ($p16^{INK4a}$ + $p19^{ARF}$) cancers rarely exhibited p53 mutant products (Gruis et al., 1995; Newcomb et al., 1995; Brenner et al., 1996; Hangaishi et al., 1996; Heinzel et al., 1996; Kinoshita et al., 1996). In 518 tumors analyzed, the mutation rates were 18% for $p16^{INK4a}$, 14% for p53, and 4% for both. *INK4a* point mutations that result in single amino acid changes in the

p16INK4a ORF were reanalyzed to determine the genetic status of the *p19ARF* ORF. Only 9 (<2%) of 405 evaluable cases harbored both p53 and *p19ARF* mutations. Since all nine cases also had alterations in *p16INK4a*, it remains possible that *p19ARF* mutation was incidental to that of *p16INK4a* in those tumors. In fact, the most common point mutation in the *p19ARF* reading frame (a P93L substitution; Quelle et al., 1995b) has been shown by us to be functionally indistinguishable from wild-type *p19ARF*. This is evidenced by the facts that the p19Arf(P93L) mutant is fully active in suppressing *Myc/RAS* and *MDM2/RAS* in the REF assay and in stabilizing p53 in the presence of high MDM2 levels (data not shown). These observations point to the need for a revisited analysis of mutations for *p19ARF*, *p16INK4a*, *p53*, and *MDM2* in the same tumor samples. Although available data (Kamijo et al., 1997; this paper) do not permit us to conclude that *p19ARF* and p53 mutations are mutually exclusive, the distinctly uncommon occurrence of comutation of *p53* and *p19ARF* supports the view that they operate through common genetic pathways for at least a significant portion of their tumor suppressor activity.

Experimental Procedures

Expression Constructs and REF Cooperation Assays

Expression constructs encoding mouse *p16Ink4a* and *p19Arf* were generated by placing the complete ORFs derived from their respective cDNAs (Schreiber-Agus et al., 1994) in the sense orientation relative to two tandemly repeated Moloney murine leukemia virus (MuLV) long terminal repeats in the pVNic vector (Schreiber-Agus et al., 1997). Expression constructs for c-*myc*, mutant H-RAS, and E1a have all been described previously (Schreiber-Agus et al., 1997), and the CMV-driven expression construct encoding the KH215 dominant-negative mutant form of p53 (Gruis et al., 1995) has been described previously. To perform the rat embryo fibroblast (REF) cooperation assays, early passage cultures of REFs were prepared and cotransfected as described previously (Schreiber-Agus et al., 1997) with DNA mixtures containing 2 μg each of the relevant expression constructs plus the corresponding amount of carrier DNA, for a total of 30 μg DNA. At 9–12 days posttransfection, foci were scored visually and confirmed by microscopic examination to be transformed morphologically. For the MEF assays, early passage MEFs were prepared from day 13.5 embryos minced and seeded into 10 cm plates. The following day, cells were split 1:3 and frozen upon reaching confluency (~24 hr). MEFs were thawed and transfected according to the REF assay protocol.

Protein Analysis

293T cells (1.4×10^6 per 10 cm plate in DME supplemented with 10% fetal bovine serum, glutamine, and antibiotics) were transfected under serum and antibiotic free conditions with 3 μg each of the appropriate expression constructs shown in Figures 2 and 3, and 80 μg of Lipofectamine reagent (GIBCO BRL). For Figure 2B, cells were metabolically labeled using the EXPRESS ^{35}S protein-labeling mix (Dupont-NEN) for 7 hr before collection. Immunoprecipitations under low-stringency conditions (1% NP-40, 10% glycerol, 10 mM NaF, 50 mM β-glycerophosphate, protease inhibitors in PBS) were performed as described previously (Schreiber-Agus et al., 1997) using anti-p53 Ab-6 conjugated beads (Calbiochem), and anti-Flag M2 (Kodak) and anti-HDM-2 Ab-1 (Calbiochem) antibodies. For high-stringency immunoprecipitations, RIPA buffer (150 mM NaCl, 1%NP-40, 0.5% deoxycholate, 0.1% SDS, and 50 mM Tris) was used. To construct the Flag epitope-tagged p19Arf construct, PCR was used to fuse in-frame Flag epitope sequences at the 3′ end of the *p19Arf* ORF, and the sequence-verified PCR product was cloned into the pcDNA (Invitrogen) expression vector. The CMV-driven human MDM2 expression construct (pCHDM1A) was provided by Arnold Levine (Princeton). The MDM2 mutant, Δ156–221, was created by standard PCR and utilization of internal restriction enzyme sites. Specifically, an XbaI site just 5′ to bases encoding amino acid 155 was ligated in-frame to a sequence-verified PCR-generated fragment containing the 5′ engineered XbaI site and beginning with amino acid residue 221 (the oligomers used are 5′-CGCCATCTAGA CCGGATCTTGATGCTGGT-3′ and 5′-CGAAGGGCCCAACATCTG-3′). The 3′ end of this PCR fragment was fused in-frame with the remainder of the *MDM2* ORF via a unique ApaI site. The final ligation was performed in the parental pCHDM1A vector in order to reconstitute the *MDM2* ORF minus sequences encoding amino acids 156–221. SAOS2 cells (5×10^6 per 10 cm plate in DME supplemented with 10% fetal bovine serum, 5% calf serum, glutamine, and antibiotics) were transfected by a modified calcium phosphate method as for the CAT assays (see below) and then processed as for 293Ts under low-stringency conditions. Untransfected 3T3DM cells were lysed in a low-stringency buffer as above. Protein (1.6 mg) was immunoprecipitated using 150 μl anti-MDM2 (2A10) (Olson et al., 1993) and protein G agarose or anti-p19Arf (4 μl) with protein A agarose for 1 hr. Western blots were probed with 2A10 1:100 to detect endogenous MDM2. The anti-p19Arf antibodies were provided by Charles Sherr (St. Jude's). For p53 degradation studies, 6×10^5 HeLa cells or H1299 cells maintained in DME supplemented with 10% fetal calf serum and antibiotics, or 5×10^6 SAOS2 cells maintained as for CAT assay were transfected by the calcium phosphate method, with 2 μg pC53SN3 (R. Tjian), 5 μg MDM2, and/or 5 μg p19Flag and harvested in RIPA buffer 24 hr after transfection. Western blots were probed with anti-p53 Ab-1 (Figure 4B), or a mixture of monoclonal p53 antibodies DO-1 and 1801 (Santa Cruz) all at 1:100 dilution (Figure 4C). For confocal analysis, 293T cells were seeded on gelatin-coated glass cover slips at a density of 130,000 cells per 2 cm well. The cells were transfected with Flag-tagged p19Arf and human MDM2 constructs as above 24 hr after seeding. Forty-eight hours posttransfection, cells were fixed in 2% paraformaldehyde for 10 min, washed in PBS, permeablized in 1% Triton X-100 for 10 min, blocked with 3% milk in PBS for 30 min, and incubated in primary antibody diluted in blocking solution overnight at 4°C. For Flag-tagged p19Arf, M2 antibody, (Kodak) was used at a concentration of 5 μg/ml. Anti-MDM2 Ab-1 (Calbiochem) was diluted 1:10. Following this incubation, cells were washed in PBS and incubated in secondary Ab for 1 hr. The secondary antibodies (Southern Biotechnology) were anti-IgG2a-Texas red for Flag and anti-IgG1-FITC for MDM2. All incubations except for primary antibody were at room temperature. Finally, cells were washed, and cover slips were mounted in 1:1 glycerol:PBS for viewing on a Bio-Rad MR600 laser-scanning confocal microscope.

TUNEL and BrdU Assays

TUNEL and BrdU incorporation assays were performed as described elsewhere (Morgenbesser et al., 1994) on 3 μM paraffin-embedded lens sections prepared as described elsewhere (Morgenbesser et al., 1994).

CAT Reporter Assays

Cultures of SAOS2 cells were maintained as above and transfected by calcium phosphate using the same amounts of DNA as in p53 degradation studies and immunoprecipitation assays, plus 2.5 μg PG13CAT, with DMSO shock, 5 hr after addition of the precipitate (Brown et al., 1993). Cells were harvested 48 hr postshocking, and CAT reporter activity was assayed by acetylation of ^{14}C-labeled chloramphenicol as reported previously (Gorman et al., 1982), except that the extracts were incubated at 37°C for 45 min, the samples were resuspended in 20 μl of ethyl acetate, and the quantities of protein assayed for CAT were approximately 30 μg per point. Transfection efficiencies were determined by addition of 2 μg of human growth hormone plasmid to each transfection point and assaying the media for human growth hormone by radioimmunoassay (Nichols Institute) just before cell lysis. Signal was quantitated using PhosphorQuant software. The reporter construct, detailed elsewhere (Bartkova et al., 1996), was the PG13-CAT construct bearing a promoter with multiple copies of the p53 consensus binding site.

Acknowledgments

The authors thank C. Sherr for the anti-p19Arf antisera, S. Efrat for the SV40 large T antigen expression construct, A. Levine for the

MDM2 and dominant-negative mutant (KH215) p53 expression constructs, D. Beach for the cDNAs encoding mouse $p16^{Ink4a}$ and $p19^{Arf}$, N. Bouck for the CAT reporter constructs, R. Tjian for the pC53SN3 wild-type p53 expression construct, S. Deb for the MDM2 deletion mutants, Jerry Shay for H1299 cells, M. Kastan and C. Finlay for helpful discussions, and Michael Cammer for confocal microscopy assistance. J. P. is a Howard Hughes Medical Institute Medical Student Research Training Fellow. N. S.-A. is a Special Fellow of the Leukemia Society of America (Grant 3712–98). N. J. L. is supported by the Medical Scientist Training Program grant. H.-W. L. is supported by the National Institutes of Health training grant. L. A. is a recipient of the James S. McDonnell Foundation Scholar award and an NIH Mentored Clinician Scientist award. C. C.-C. is supported by grants CA47538, CA47179, and CADK97650 from the National Institutes of Health. R. A. D. is supported by grants (R01HD28317, R01EY09300, and R01EY11267) from the National Institutes of Health, as well as the Irma T. Hirschl Award. The Albert Einstein Cancer Center Core grant P30CA13330 support is acknowledged.

Received January 5, 1998; revised February 10, 1998.

References

Alland, L., Muhle, R., Hou, H., Jr., Potes, J., Chin, L., Schreiber-Agus, N., and DePinho, R.A. (1997). Role for N-CoR and histone deacetylase in Sin3-mediated transcriptional repression. Nature *387*, 49–55.

Barak, Y., Gottlieb, E., Juven-Gershon, T., and Oren, M. (1994). Regulation of *mdm2* expression by p53: alternative promoters produce transcripts with nonidentical translation potential. Genes Dev. *8*, 1739–1749.

Bartkova, J., Lukas, J., Guldberg, P., Alsner, J., Kirkin, A.F., Zeuthen, J., and Bartek, J. (1996). The p16-cyclin D/Cdk4-pRb pathway as a functional unit frequently altered in melanoma pathogenesis. Cancer Res. *56*, 5475–5483.

Brenner, A., Paladugu, A., Wang, H., Olopade, O.I., Dreyling, M.F., and Aldaz, C.M. (1996). Preferential loss of expression of $p16^{INK4a}$ rather than $p19^{ARF}$ in breast cancer. Clin. Cancer Res. *2*, 1993–1998.

Brown, D.R., Deb, S., Munoz, R., Subler, M., and Deb, S.P. (1993). The tumor suppressor p53 and the oncoprotein simian virus 40 T antigen bind to overlapping domains on the MDM2 protein. Mol. Cell. Biol. *13*, 6849–6857.

Cahilly-Snyder, L., Yang-Feng, T., Francke, U., and George, D.L. (1987). Molecular analysis and chromosomal mapping of amplified genes isolated from a transformed mouse 3T3 cell line. Somat. Cell Mol. Genet. *13*, 235–244.

Chen, J.D., Lin, J.Y., and, Levine, A.J. (1995). Regulation of transcription functions of the p53 tumor suppressor by the *mdm-2* oncogene. Mol. Med. *1*, 141–142.

Chin, L., Pomerantz, J., Polsky, D., Jacobson, M., Cohen, C., Cordon-Cardo, C., Horner, J.W., and DePinho, R.A. (1997). Cooperative effects of *INK4a* and *ras* in melanoma susceptibility in vivo. Genes Dev. *11*, 2822–2834.

Cordon-Cardo, C. (1995). Mutations of cell cycle regulators. Biological and clinical implications for human neoplasia. Am. J. Pathol. *147*, 545–560.

Crook, T., Marston, N.J., Sara, E.A., and Vousden, K.H. (1994). Transcriptional activation by p53 correlates with suppression of growth but not transformation. Cell *79*, 817–827.

El-Deiry, W.S., Tokino, T., Velculescu, V.E., Levy, D.B., Parsons, R., Trent, J.M., Lin, D., Mercer, W.E., Kinzler, K.W., and Vogelstein, B. (1993). WAF1, a potential mediator of p53 tumor suppression. Cell *75*, 817–825.

Eliyahu, D., Michalovite, D., Eliyahu, S., Pinhasi-Kimhi, O., and Oren, M. (1989). Wild-type p53 can inhibit oncogene-mediated focus formation. Proc. Natl. Acad. Sci. USA *86*, 8763–8767.

Elledge, S.J., Winston, J., and Harper, J.W. (1996). A question of balance: the role of cyclin-kinase inhibitors in development and tumorigenesis. Trends Biochem. Sci. *6*, 388–392.

Fakharzadeh, S.S., Trusko, S.P., and George, D.L. (1997). Tumorigenic potential associated with enhanced expression of a gene that is amplified in a mouse tumor cell line. EMBO J. *10*, 1565–1569.

Fanning, E. (1992). Simian virus 40 large T antigen: the puzzle, the pieces, and the emerging picture. J. Virol. *66*, 1289–1293.

Finlay, C.A. (1993). The *mdm-2* oncogene can overcome wild-type p53 suppression of transformed cell growth. Mol. Cell. Biol. *13*, 301–306.

Finlay, C.A., Hinds, P.W., and Levine, A.J. (1989). The p53 protooncogene can act as a suppressor of transformation. Cell *57*, 1083–1093.

Gorman, C.M., Moffat, L.F., and Howard, B.H. (1982). Recombinant genomes which express chloramphenicol acetyltransferase in mammalian cells. Mol. Cell. Biol. *2*, 1044–1051.

Gottlieb, T.M., and Oren, M. (1996). p53 in growth control and neoplasia. Biochim. Biophys. Acta. *1287*, 77–102.

Gruis, N.A., Weaver-Feldhaus, J., Liu, Q., Frye, C., Eeles, R., Orlow, I., Lacombe, L., Ponce-Castaneda, V., Lianes, P., Latres, E., et al. (1995). Genetic evidence in melanoma and bladder cancers that p16 and p53 function in separate pathways of tumor suppression. Am. J. Pathol. *146*, 1199–1206.

Hangaishi, A., Ogawa, S., Imamura, N., Miyawaki, S., Miura, Y., Uike, N., Shimazaki, C., Emi, N., Takeyama, K., Hirosawa, S., et al. (1996). Inactivation of multiple tumor-suppressor genes involved in negative regulation of the cell cycle, *MTS1/p16^{INK4A}/CDKN2*, *MTS2/p15INK4B*, *p53*, and *Rb* genes in primary lymphoid malignancies. Blood *87*, 4949–4958.

Haupt, Y., Maya, R., Kazaz, A., and Oren, M. (1997). Mdm2 promotes the rapid degradation of p53. Nature *387*, 296–299.

Hawley-Nelson, P., Vousden, K.H., Hubbert, N.L., Lowy, D.R., and Schiller, J.T. (1989). HPV16 E6 and E7 proteins cooperate to immortalize human foreskin keratinocytes. EMBO J. *8*, 3905–3910.

Heinzel, P.A., Balaram, P., and Bernard, H.U. (1996). Mutations and polymorphisms in the p53, p21 and p16 genes in oral carcinomas of Indian betel quid chewers. Int. J. Cancer *68*, 420–423.

Henning, W., Rohaly, G., Kolzau, T., Knippschild, U., Maacke, H., and Deppert, W. (1997). MDM2 is a target of simian virus 40 in cellular transformation and during lytic infection. J. Virol. *71*, 7609–7618.

Hollstein, M., Sidransky, D., Vogelstein, B., and Harris, C.C. (1991). p53 mutations in human cancers. Science *253*, 49–53.

Jacks, T. (1994). Tumor spectrum analysis in p53-mutant mice. Curr. Biol. *4*, 1–7.

Jones, S.N., Roe, A.E., Donehower, L.A., and Bradley, A. (1995). Rescue of embryonic lethality in Mdm2-deficient mice by absence of p53. Nature *378*, 206–208.

Kamb, A., Gruis, N.A., Weaver-Feldhaus, J., Liu, Q., Harshman, K., Tavtigian, S.V., Stockert, E., Day, R.S., III, Johnson, B.E., and Skolnick, M.H. (1994). A cell cycle regulator potentially involved in genesis of many tumor types. Science *264*, 436–440.

Kamijo, T., Zindy, F., Roussel, M.F., Quelle, D.E., Downing, J.R., Ashmun, R.A., Grosveld, G., and Sherr, C.J. (1997). Tumor suppression at the mouse *INK4a* locus mediated by the alternative reading frame product $p19^{ARF}$. Cell *91*, 649–659.

Kinoshita, I., Dosaka-Akita, H., Mishina, T., Akie, K., Nishi, M., Hiroumi, H., Hommura, F., and Kawakami, Y. (1996). Altered $p16^{INK4}$ and retinoblastoma protein status in non-small cell lung cancer: potential synergistic effect with altered p53 protein on proliferative activity. Cancer Res. *56*, 5557–5562.

Ko, L.J., and Prives, C. (1996). p53: puzzle and paradigm. Gene Dev. *10*, 1054–1072.

Kubbutat, M.H., Jones, S.N., and Vousden, K.H. (1997). Regulation of p53 stability by Mdm2. Nature *387*, 299–303.

Kussie, P.H., Gorina, S., Marechal, V., Elenbaas, B., Moreau, J., Levine, A.J., and Pavletich, N.P. (1996). Structure of the MDM2 oncoprotein bound to the p53 tumor suppressor transactivation domain. Science *274*, 948–953.

Lahoz, E.G., Xu, L., Schreiber-Agus, N., and DePinho, R.A. (1997). Suppression of Myc, but not E1a, transformation activity by Max-associated proteins, Mad and Mxi1. Proc. Natl. Acad. Sci. USA *91*, 5503–5507.

Land, H., Parada, L.F., and Weinberg, R.A. (1983). Tumorigenic conversion of primary embryo fibroblasts requires at least two cooperating oncogenes. Nature *304*, 596–602.

Levine, A.J. (1997). p53, the cellular gatekeeper for growth and division. Cell *88*, 323–331.

Levine, A.J., Momand, J., and Finlay, C.A. (1991). The p53 tumor suppressor gene. Nature *351*, 453–456.

Lukas, J., Perry, D., Aagaard, L., Mann, D.J., Bartkova, J., Strauss, M., Peters, G., and Bartek, J. (1995). Retinoblastoma-protein-dependent cell-cycle inhibition by the tumour suppressor p16. Nature *375*, 503–506.

Mahon, K.A., Chepelinsky, A.B., Khillan, J.S., Overbeek, P.A., Piatigorsky, J., and Westphal, H. (1987). Oncogenesis of the lens in transgenic mice. Science *235*, 1622–1628.

Medema, R.H., Herrera, R.E., Lam, F., and Weinberg, R.A. (1995). Growth suppression by p16 *Ink4* requires functional retinoblastoma protein. Proc. Natl. Acad. Sci. USA *92*, 6289–6293.

Momand, J., Zambetti, G.P., Olson, D.C., George, D., and Levine, A.J. (1992). The *mdm-2* oncogene product forms a complex with the p53 protein and inhibits p53-mediated transactivation. Cell *69*, 1237–1245.

Morgenbesser, S.D., Williams, B.O., Jacks, T., and DePinho, R.A. (1994). p53-dependent apoptosis produced by Rb-deficiency in the developing mouse lens. Nature *371*, 72–74.

Munger, K., Phelps, W.C., Bubb, V., Howley, P.M., and Schlegel, R. (1989). The E6 and E7 genes of the human papillomavirus type 16 together are necessary and sufficient for transformation of primary human keratinocytes. J. Virol. *63*, 4417–4421.

Newcomb, E.W., Rao, L.S., Giknavorian, S.S., and Lee, S.Y. (1995). Alterations of multiple tumor suppressor genes (*p53* (*17p13*), $p16^{INK4}$ (*9p21*), and *DBM* (*13q14*) in B-cell chronic lymphocytic leukemia. Mol. Carcinog. *14*, 141–146.

Oliner, J.D., Kinzler, K.W., Meltzer, P.S., George, D.L., and Vogelstein, B. (1992). Amplification of a gene encoding a p53-associated protein in human sarcomas. Nature *358*, 80–83.

Oliner, J.D., Pietenpol, J.A., Thiagalingam, S., Gyuris, J., Kinzler, K.W., and Vogelstein, B. (1993). Oncoprotein MDM2 conceals the activation domain of tumour suppressor p53. Nature *362*, 857–860.

Olson, D.C., Marechal, V., Momand, J., Chen, J., Romocki, C., and Levine, A.J. (1993). Identification and characterization of multiple mdm-2 proteins and mdm-2-p53 protein complexes. Oncogene *8*, 2353–2360.

Pietenpol, J.A., Tokino, T., Thiagalingam, S., El-Deiry, W.S., Kinzler, K.W., and Vogelstein, B. (1994). Sequence-specific transcriptional activation is essential for growth suppression by p53. Proc. Natl. Acad. Sci. USA *91*, 1998–2002.

Quelle, D.E., Ashmun, R.A., Hannon, G.J., Rehberger, P.A., Trono, D., Richter, H., Walker, C., Beach, D., Sherr, C.J., and Serrano, M. (1995a). Cloning and characterization of murine $p16^{INK4a}$ and $p15^{INK4b}$ genes. Oncogene *11*, 635–645.

Quelle, D.E., Zindy, F., Ashmun, R.A., and Sherr, C.J. (1995b). Alternative reading frames of the *INK4a* tumor suppressor gene encode two unrelated proteins capable of inducing cell cycle arrest. Cell *83*, 993–1000.

Quelle, D.E., Cheng, M., Ashmun, R.A., and Sherr, C.J. (1997). Cancer-associated mutations at the *INK4a* locus cancel cell cycle arrest by p16INK4a but not by the alternative reading frame protein p19ARF. Proc. Natl. Acad. Sci. USA *94*, 669–673.

Schreiber-Agus, N., Chin, L., Chen, K., Torres, R., Thomson, C.T., Sacchettini, J.C., and DePinho, R.A. (1994). Evolutionary relationships and functional conservation among vertebrate Max-associated proteins: the zebrafish homolog of Mxi1. Oncogene *9*, 3167–3177.

Schreiber-Agus, N., Chin, L., Chen, K., Torres, R., Rao, G., Guida, P., Skoultchi, A.I., and DePinho, R.A. (1995). An amino-terminal domain of Mxi1 mediates anti-Myc oncogenic activity and interacts with a homolog of the yeast transcriptional repressor SIN3. Cell *80*, 777–786.

Schreiber-Agus, N., Chin, L., Chen, K., Torres, R., Rao, G., Guida, P., Skoultchi, A.I., and DePinho, R.A. (1997). An amino-terminal domain of Mxi1 mediates anti-Myc oncogenic activity and interacts with a homolog of the yeast transcriptional repressor SIN3. Cell *80*, 777–786.

Serrano, M., Hannon, G.J., and Beach, D. (1993). A new regulatory motif in cell cycle control causing specific inhibition of cyclin D/cdk4. Nature *366*, 704–707.

Serrano, M., Gomez-Lahoz, E., DePinho, R.A., Beach, D., and Bar-Sagi, D. (1995). Inhibition of ras-induced proliferation and cellular transformation by $p16^{INK4}$. Science *267*, 249–252.

Serrano, M., Lee, H., Chin, L., Cordon-Cardo, C., Beach, D., and DePinho, R.A. (1996). Role of the *INK4a* locus in tumor suppression and cell mortality. Cell *85*, 27–37.

Sherr, C.J. (1996). Cancer cell cycles. Science *274*, 1672–1676.

Symonds, H., Krall, K., Remington, L., Saenz-Robles, M., Lowe, S., Jacks, R., and Van Dyke, T. (1994). p53-dependent apoptosis suppresses tumor growth and progression in vivo. Cell *78*, 703–711.

Thut, C.J., Goodrich, J.A., and Tjian, R. (1997). Repression of p53-mediated transcription by MDM2: a dual mechanism. Genes Dev. *11*, 1974–1986.

Van Dyke, T.A. (1994). Analysis of viral-host protein interactions and tumorigenesis in transgenic mice. Semin. Cancer Biol. *5*, 47–60.

Weinberg, R.A. (1995). The retinoblastoma protein and cell cycle control. Cell *81*, 323–330.

Williams, B.O., Remington, L., Albert, D.M., Mukai, S., Bronson, R.T., and Jacks, T. (1994). Cooperative tumorigenic effects of germline mutations in Rb and p53. Nature Genet. *7*, 480–484.

Xiao, Z.X., Chen, J., Levine, A.J., Modjtahedi, N., Xing, J., Sellers, W.R., and Livingston, D.M. (1995). Interaction between the retinoblastoma protein and the oncoprotein MDM2. Nature *375*, 694–698.

Zhang, Y., Xiong, Y., and Yarbrough, W.G. (1998). ARF promotes MDM2 degradation and stabilizes p53: *ARF-INK4a* locus deletion impairs both the Rb and p53 tumor suppression pathways. Cell *92*, this issue, 725–734.

Zuo, L., Weger, J., Yang, B., Goldstein, A.M., Tucker, M.A., Walker, G.J., Hayward, N., and Dracopoli, N.C. (1996). Germline mutations in the $p16^{INK4a}$ binding domain of CDK4 in familial melanoma. Nature Genet. *12*, 97–99.